Catal Lett (2010) 140:55–64
DOI 10.1007/s10562-010-0423-z

Chemoselective Hydrogenation of Cinnamaldehyde over Pd/CeO_2–ZrO_2 Catalysts

S. Bhogeswararao · D. Srinivas

Received: 3 June 2010 / Accepted: 30 July 2010 / Published online: 14 August 2010

Abstract Selective hydrogenation of cinnamaldehyde over Pd (2 wt%) supported on CeO_2, ZrO_2 and CeO_2–ZrO_2 catalysts is reported for the first time. In general, the olefinic (C=C) group of cinnamaldehyde is preferentially hydrogenated compared to the carbonyl (C=O) group. This selectivity preference could, however, be altered or reversed by adding alkali additives to the catalyst. The influence of additive on the structure and redox properties of the active sites and correlation of that with selective hydrogenation activity is investigated.

Keywords Hydrogenation · Cinnamaldehyde · α, β-Unsaturated aldehyde · Ceria–zirconia · Palladium catalyst

1 Introduction

Selective hydrogenation of α, β-unsaturated aldehydes is one of the most important areas in catalysis research [1]. Cinnamaldehyde is a vinyologue of benzaldehyde. In such compounds, hydrogenation can occur either at olefinic (C=C) or carbonyl (C=O) groups. While the former leads to saturated aldehydes of industrial and biological importance, the latter results in unsaturated alcohols (Scheme 1). All these selective hydrogenation products of cinnamaldehyde are widely used in the perfumery industry. Recently hydrocinnamaldehyde was found be an important intermediate in the preparation of pharmaceuticals used in the treatment of HIV [2]. Supported Pt, Ru, Co, Au and Ir catalysts [3–8] were reported to selectively hydrogenate the carbonyl group resulting in cinnamyl alcohol. On the contrary, supported Pd catalysts were selective for hydrogenation of olefinic group resulting in hydrocinnamyl aldehyde [9]. In view of the industrial importance of the hydrogenation products, design and development of more efficient and selective catalysts is still remaining as a challenging task. For this, a detailed study revealing the influence of the nature of metal and support metal-interaction is essential. We report here, for the first time, a preliminary study on the catalytic activity of Pd (2 wt%) supported on CeO_2, ZrO_2 and CeO_2–ZrO_2. The influence of various reaction parameters and in particular, alkali (NaOH) addition on product selectivity is investigated. By incorporation of Zr ions into ceria lattice, the redox behaviour of the ceria is enhanced [10]. Zirconia incorporation also increases the thermal stability of CeO_2 and improves the metal–CeO_2 interactions. CeO_2–ZrO_2-supported Pd has been used as three-way catalysts [11–16], in natural gas combustion [17], total oxidation of hydrocarbons [18], methanol decomposition [19], vapor phase hydrogenation of phenol [20] and in several other reactions [21]. We report here the chemoselective hydrogenation activity of these novel catalysts.

2 Experimental

2.1 Catalyst Preparation

2.1.1 CeO_2–ZrO_2

CeO_2–ZrO_2 composites were prepared by co-precipitation method [3]. $Ce(NO_3)_3{\cdot}6H_2O$ (7.35 g, Semco) and $ZrO(NO_3)_2{\cdot}xH_2O$ (2.8 g, Loba Chemie) were dissolved separately in distilled water (168 and 120 mL, respectively).

S. Bhogeswararao · D. Srinivas (✉)
Catalysis Division, National Chemical Laboratory, Pune 411 008, India
e-mail: d.srinivas@ncl.res.in

Scheme 1 Hydrogenation products of cinnamaldehyde

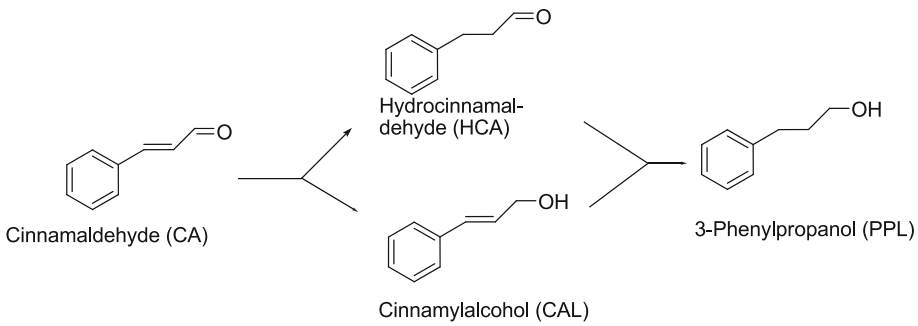

These solutions were mixed together and added drop-wise to a continuously stirred 0.1 M aq. solution (1 L) of NaOH taken in a 2 L round bottom flask, placed in an oil bath. Stirring was continued for 3 h. During addition, the temperature of the flask was maintained at 80 °C and pH at 10. The cations were precipitated in the form of their hydroxides. The mixture was digested at 80 °C for another 3 h and then cooled to 25 °C. The precipitate was separated, washed with copious amounts of distilled water until all the Na^+ ions were removed. It was then air-dried, powdered and calcined at 450 °C, for 2.5 h, to get the final product. The CeO_2 to ZrO_2 molar ratios in the composites were 1:1, 1:2 and 1:4. The Na content in the samples is below the detection limit of inductively couple plasma (ICP) technique. "Neat" ceria and "neat" zirconia supports were also prepared by the precipitation method.

2.1.2 CeO_2–ZrO_2-Supported Pd Catalysts

Pd (2 wt%) supported on CeO_2–ZrO_2 was prepared by dry-impregnation method. In a typical preparation, 0.570 g of tetraamminepalladium(II) nitrate [$Pd(NH_3)_4(NO_3)_2$, 10 wt% solution in water, Aldrich] was added drop-wise to 1 g of CeO_2–ZrO_2 taken in a beaker. It was mixed thoroughly at 25 °C, dried at 120 °C for 5 h till all the water evaporated and then, calcined at 400 °C for 2 h. Pd (2 wt%)/CeO_2 and Pd (2 wt%)/ZrO_2 catalysts were prepared in a similar manner.

2.1.3 Alkali Impregnated CeO_2–ZrO_2-Supported Pd Catalysts

In a typical synthesis, 0.262 g of NaOH dissolved in 1 mL of water and 0.570 g of 10 wt% aqueous solution of tetraamminepalladium(II) nitrate were added slowly to 1 g of CeO_2–ZrO_2 while mixing thoroughly at 25 °C. The slurry was dried at 120 °C for 5 h till the water got evaporated. It was then, calcined at 400 °C for 2 h.

2.2 Characterization Techniques

Crystallinity and phase purity of the samples were determined from X-ray diffractograms (XRD) recorded on a Xpert Pro PANalytical X-ray diffractometer with Ni-filtered Cu Kα radiation (40 kV, 30 mA) in the 2θ range of 10–80° at a scan rate of 2.3°/min. The specific surface area (BET) of the samples was determined using a NOVA 1200 Quanta Chrome instrument. The micropore volume was estimated from the t-plot and the pore diameter was estimated using the Barret-Joyner-Halenda (BJH) model. Morphological characteristics of the samples were determined using a high resolution transmission electron microscope (HRTEM, JEOL, model 1200 EX) operating at 100 kV.

X-ray photoelectron spectra (XPS) of the samples were acquired on a VG Microtech Multilab ESCA 3000 with Mg Kα radiation (hν = 1253.6 eV). Base pressure in the analysis chamber was maintained at 3–6 $\times$ 10^{-10} mbar. The peak corresponding to carbon 1s (at 284.2 eV) was taken as the reference in estimating the binding energy (BE) values of various elements in the catalyst. The error in BE values is $\pm$0.1 eV. Samples were prepared by pressing the powders into pellets. In order to accelerate outgassing and remove C from the surface, samples were heated at 450 °C for 2 h in flowing O_2 before performing the XPS measurements. The measurements included a survey spectrum and the Ce 3d, Zr 3d and Pd 3d core-level spectra, which were analyzed following the standard procedures.

Temperature-programmed reduction experiments were carried on a Micromeritics Auto Chem 2910 instrument: 0.1 g of the catalyst was placed in a quartz tube and treated with a O_2 (22%)–He (78%) gas mixture (30 cm^3/min) at 250 °C for 2 h. A gas mixture of H_2 (5%)–Ar (95%) was then passed (50 cc^3/min) through the quartz reactor at 25 °C for 1 h. The temperature was raised to 950 °C at a heating rate of 5°/min and held at 950 °C for 0.5 h. The amount of hydrogen consumed was estimated and the reduction capacity of the catalyst was determined. A standard CuO powder was used to calibrate the amount of H_2 consumption.

The type and density of the acid sites were determined by diffuse reflectance infrared Fourier transform (DRIFT) spectroscopy of adsorbed pyridine and temperature-programmed ammonia desorption (NH_3-TPD) techniques. In DRIFT measurements, the samples were initially activated

at 450 °C. The temperature was brought down to 50 °C and pyridine was adsorbed. Then, the temperature of the sample was raised and held at a desired value (100 °C) for 0.5 h before starting the measurements (spectral resolution = 2 cm^{-1}; number of scans = 200). Difference FTIR spectra were obtained by subtracting the spectrum of the catalyst from that of the sample adsorbed with pyridine.

NH_3-TPD measurements performed on a Micromeritics AutoChem 2910 instrument. In a typical experiment, 0.1 g of catalyst was taken in a U-shaped, flow-thru, quartz sample tube. Prior to measurements, the catalyst was pretreated in He (30 cm^3/min) at 700 °C for 1 h. A mixture of NH_3 in He (10%) was passed (30 cm^3/min) at 25 °C for 1 h. Then, the sample was, subsequently flushed with He (30 cm^3/min) at 100 °C for 1 h. The TPD measurements were carried out in the range 100–800 °C at a heating rate of 10 °C/min. Ammonia concentration in the effluent was monitored with a gold-plated, filament thermal conductivity detector. The amount of desorbed ammonia was determined based on the area under the peak.

2.3 Reaction Procedure: Hydrogenation of Cinnamaldehyde

Prior to reactions, the catalyst was reduced under a flow of hydrogen (30 mL/min) at 200 °C for 2 h. Upon reduction, the color of the catalyst changed from dark brown to black. It was cooled to 25 °C. Without exposing to atmosphere, 0.05 g of the reduced catalyst was transferred into a Parr reactor (300 mL) containing cinnamaldehyde (4 g) and solvent (40 mL). The reactor was initially flushed and then pressurized with hydrogen to a desired value (2, 5, 10 or 20 bar). The temperature of the reactor was also raised to a desired value (50, 80, 120 or 150 °C) and the reaction was conducted while stirring (500 revolutions per minute) for 8 h. Samples were collected at intermittent times, diluted with the solvent and then analyzed and quantified by gas chromatographic technique (Varian 3400; CP-SIL8CB column; 30 m-long and 0.53 mm-i.d.). The products were identified by GC-MS (Shimadzu GCMS-QP5050A; HP-5 column; 30 m-long × 0.25 mm i.d. × 0.25 μm thickness).

3 Results and Discussion

3.1 Structural and Textural Properties

3.1.1 X-Ray Diffraction

The ceria–zirconia mixed oxides are formed in different crystalline structures depending on their chemical composition. According to the $Ce_{1-x}Zr_xO_2$ phase diagram, for $x \leq 0.15$ a cubic fluorite-type phase is formed, while for $x \geq 0.85$, a monoclinic phase is produced [22]. At intermediate compositions, various phases (t, t′, t″, κ and t*) have been identified [22–24]. Oxygen deficient structures, such as the pyrochlore structure ($A_2B_2X_7$) may also be formed [25–29]. For ceria–zirconia mixed oxides, the pyrochloric structure is generally reported to be formed under severe reduction conditions. However, there is an evidence of its formation even during low temperature reduction of the sample [29]. In other words, the ceria–zirconia material exhibit complex structural characteristics. Neat ceria of the present study showed XRD peaks in the 2θ range of 28–80° indicating a distinct, cubic, fluorite structure [30]. On the contrary, the CeO_2–ZrO_2 composites exhibited XRD pattern typical of a mixture of cubic and tetragonal phases with the former being more predominant (Fig. 1; the peaks due to the tetragonal phase are marked by asterisk). Recently, Li et al. [31] have also reported such a mixed crystallite phase in CeO_2–ZrO_2 materials prepared by calcining at lower temperatures (<500 °C). In the materials prepared by us, the presence of pyrochloric structure was not detected. The unit cell parameter of the cubic phase (a_{cubic}) of CeO_2–ZrO_2 is smaller (0.537 nm) than CeO_2 (0.542 nm), suggesting the formation of a CeO_2–ZrO_2 solid solution [note: ionic radius of Zr^{4+} (0.084 nm) is smaller than that of Ce^{4+} (0.097 nm)/Ce^{3+} (0.112 nm)] [32]. Palladium and sodium impregnation did not alter the structure except for shift in peaks to higher 2θ value by 0.1–0.3°. At 2 wt% of Pd loading, no separate PdO phase was detected indicating that it is highly dispersed. Representative XRD profiles of CeO_2–ZrO_2, Pd/CeO_2–ZrO_2 and Na–Pd/CeO_2–ZrO_2 are depicted in Fig. 1. The average crystallite size of the materials was determined from the linewidth of the XRD peak corresponding to (111) reflection (2θ ≈ 28.7°) using

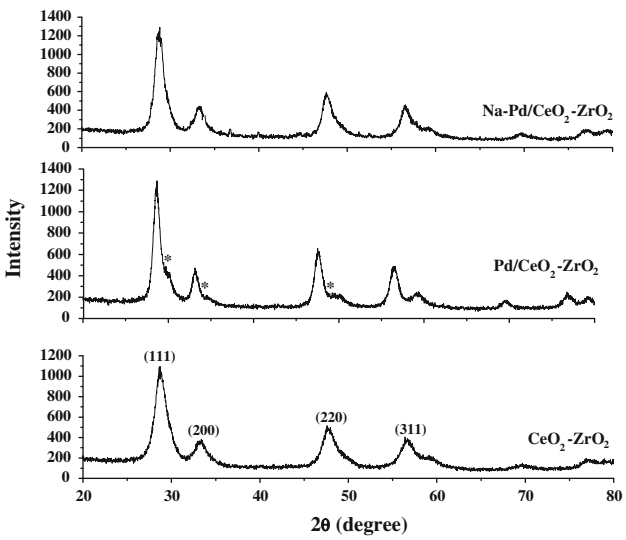

Fig. 1 X-ray diffractograms of CeO_2–ZrO_2 (1:1 M ratio) and supported Pd catalysts

Table 1 Physicochemical properties of CeO_2–ZrO_2-supported Pd catalysts

Sample	XRD		N_2 adsorption–desorption			Acidity (NH_3-TPD, mmol/g)	H_2 uptake–Pd (TPR, mmol/g)
	Lattice parameter (a_{cubic}, nm)	Average crystallite size (nm)	S_{BET} (m^2/g)	Pore volume (cm^3/g)	Average pore diameter (nm)		
CeO_2	0.542	6.9	–	–	–	–	
ZrO_2	0.512	11.5	–	–	–	–	
CeO_2–ZrO_2	0.537	6.7	115	0.17	6.1	0.179	
Pd (2 wt%)/CeO_2	0.540	10.0	–	–	–	0.231	
Pd (2 wt%)/ZrO_2	0.510	11.1	–	–	–	0.390	
Pd (2 wt%)/CeO_2–ZrO_2 (1:1)	0.538	10.6	65	0.11	7.2	0.308	0.076
Na–Pd (2 wt%)/CeO_2–ZrO_2 (1:1)	0.538	8.5	121	0.14	4.3	0.034	0.583

Debye-Scherrer equation (Table 1). It varied for different supports in the order: ZrO_2 (11.5 nm) > CeO_2 (6.9 nm) > CeO_2–ZrO_2 (6.7 nm) indicating that zirconia incorporation renders materials with low crystallite size. The crystallite size of CeO_2–ZrO_2-supported Pd was higher (10.6 nm) than the corresponding support oxide (6.7 nm, respectively). Alkali impregnation (Na–Pd/CeO_2–ZrO_2) decreased the crystallite size to 8.5 nm.

3.1.2 N_2 Adsorption–Desorption

The textural properties of CeO_2–ZrO_2, Pd/CeO_2–ZrO_2 and Na–Pd/CeO_2–ZrO_2 were determined by N_2 adsorption–desorption technique (Fig. 2; Table 1). All these materials showed typical type IV isotherms with H3 hysteresis loops. The specific surface area (S_{BET}) and pore volume of supported Pd catalysts are lower (65 m^2/g and 0.11 cm^3/g, respectively) than those of the support composite oxide (115 m^2/g and 0.17 cm^3/g, respectively). When sodium was also present the material exhibited highest S_{BET} (121 m^2/g). However, the average pore diameter of it was lower (4.3 nm) than CeO_2–ZrO_2 (6.1 nm) and Pd/CeO_2–ZrO_2 (7.2 nm). It is worth noting that the variation in S_{BET} (obtained from N_2 adsorption–desorption measurements) follows the variation in crystallite size of these materials (determined from XRD studies).

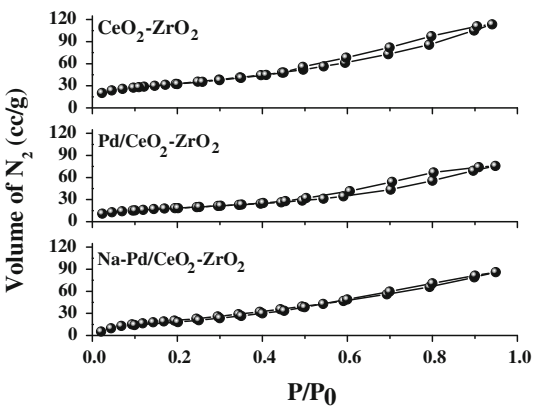

Fig. 2 N_2 adsorption–desorption isotherms of CeO_2–ZrO_2 (1:1 M ratio) and supported Pd catalysts

3.1.3 High Resolution Transmission Electron Microscopy

Representative HRTEM images of Pd/CeO_2, Pd/ZrO_2 and Pd/CeO_2–ZrO_2 are shown in Fig. 3. Palladium is in a dispersed state on CeO_2–ZrO_2 support. Agglomeration of particles was detected on neat ceria and zirconia supports. In spite of the fact that HRTEM usually only measures a small area of the sample, it is interesting to note that the crystallite size of the support (5–12 nm) estimated with HRTEM) agrees well with that determined using XRD. CO chemisorption could provide more information on metal dispersion. However, these experiments could not be done due to lack of this facility.

3.1.4 X-Ray Photoelectron Spectroscopy

Representative X-ray photoelectron spectra of Pd/CeO_2–ZrO_2 catalysts in Pd 3d region are shown in Fig. 4. The binding energy values are reported in Table 2. The binding energies of Pd^0, Pd^{2+} and Pd^{4+} states are 335 and 340.6, 337.5 and 342.9, and 338.4 and 343.5 eV, respectively corresponding to the $3d_{5/2-3/2}$ spin–orbit doublet [33–36]. The binding energy of Zr 3p also falls in the same range. Therefore, the B.E. peaks of Zr 3p overlap with those of Pd 3d. From the estimated binding energy values (Table 2) it is concluded that Pd on CeO_2–ZrO_2 is in a +2 oxidation state. The binding energy value of Pd ($3d_{5/2}$) on pure ZrO_2 is higher than that observed over pure CeO_2 support consistent with the facile reducibility of the latter than the former support. The $3d_{5/2}$ peak of Pd in Na–Pd/CeO_2–ZrO_2 appeared at lower binding energy value (336.5 eV) than that of Pd/CeO_2–ZrO_2 (336.8 eV) revealing that Pd in the

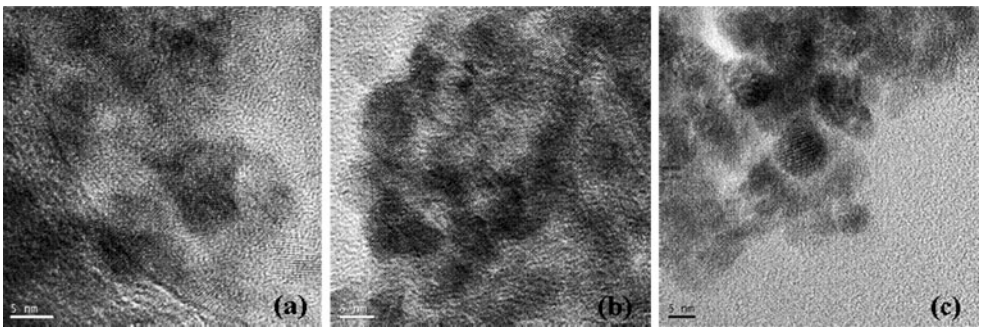

Fig. 3 High-resolution transmission electron micrographs: **a** Pd (2 wt%)/CeO_2, **b** Pd (2 wt%)/ZrO_2, and **c** Pd (2 wt%)/CeO_2–ZrO_2 (Ce:Zr molar ratio = 1:1)

Fig. 4 XPS of Pd 3d region of supported palladium catalysts

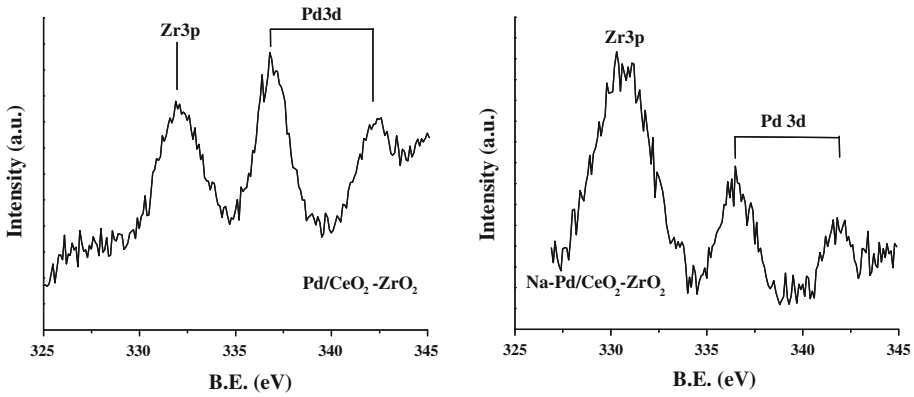

Table 2 Binding energy values (in eVs) for supported Pd catalysts

Sample	Pd $3d_{5/2}$	Ce $3d_{5/2}$	Zr $3d_{5/2}$	Na 1s
Pd/CeO_2	336.4	881.3	–	–
Pd/ZrO_2	337.9	–	181.5	–
Pd/CeO_2–ZrO_2	336.8	881.0	181.3	–
Na–Pd/CeO_2–ZrO_2	336.5	881.2	181.0	1070.1

former is in a reduced $+(2-\delta)$ oxidation state while that in the latter is in a "formal" +2 oxidation state. In other words, alkali affected the electronic structure of Pd. The peaks corresponding to Pd in Na–Pd/CeO_2–ZrO_2 are broader than those for Pd/CeO_2–ZrO_2 due to the presence of different metal oxidation states (+2 and $+(2-\delta)$). This led to differences in the relative intensity of Zr and Pd peaks in these two samples (Fig. 4). The B.E. values of Ce $3d_{5/2}$ and Zr $3d_{5/2}$ are also included in Table 2 and are consistent with the reported values [33].

3.1.5 Acidic Properties: DRIFT Spectroscopy of Adsorbed Pyridine and NH_3-TPD

CeO_2–ZrO_2 is a weakly acidic oxide. The nature and type of acid sites on CeO_2–ZrO_2 were determined by DRIFT spectroscopy using pyridine as probe molecule (Fig. 5). The sample showed IR peaks of adsorbed pyridine at 1592, 1575, 1484 and 1440 cm^{-1} (Fig. 5). While the peaks at 1592 and 1440 cm^{-1} are attributed to H-bonded pyridine, those at 1575 and 1484 cm^{-1} are corresponded to pyridine-coordinated to weak Lewis acid sites [37]. It is known that strong Lewis acid sites show adsorbed pyridine-IR peaks at 1623 and 1455 cm^{-1} and Brönsted sites at 1639 and 1546 cm^{-1}. However, these peaks are not observed in the spectrum of CeO_2–ZrO_2 indicating that such strong acidic sites are absent. The pyridine-IR peaks broadened and decreased in intensity as the desorption temperature increased from 200 to 400 °C (Fig. 5). At higher temperatures (ca., 400 °C) strong additional peaks appeared at 1540 and 1580 cm^{-1}, the origin of which is not clear at this point of time.

The number of acidic sites on CeO_2–ZrO_2 and supported Pd catalysts were quantified by NH_3-TPD measurements (Fig. 6; Table 1). CeO_2–ZrO_2 showed a broad desorption peak in the temperature region 100–500 °C (Fig. 6, right panel). Based on the knowledge gained from pyridine-IR studies, this broad NH_3 desorption is attributed to surface acidic hydroxyl and weak Lewis acid (Ce and Zr) sites. In the case of Pd catalysts a shoulder peak was also observed at around 110–150 °C which could be attributed to NH_3 desorption from PdO species (Fig. 6). The amount of NH_3 desorbed from different supported Pd catalysts decreased in

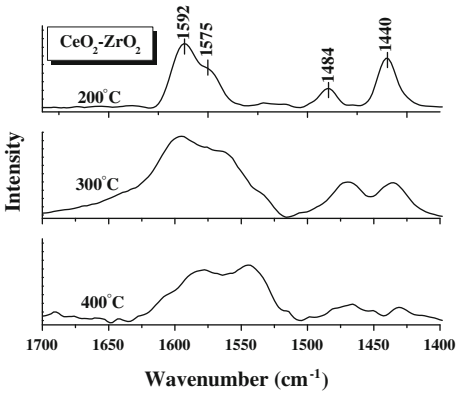

Fig. 5 Pyridine-IR of CeO_2–ZrO_2 support

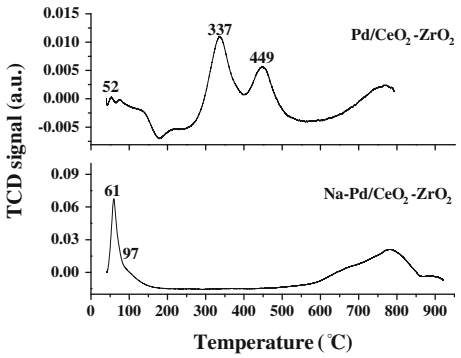

Fig. 7 H_2—temperature-programmed reduction of supported Pd catalysts

the following order: Pd/ZrO_2 (0.390 mmol/g) > Pd/CeO_2–ZrO_2 (0.308 mmol/g) > Pd/CeO_2 (0.231 mmol/g). The amount of NH_3 desorbed from support CeO_2–ZrO_2 was found to be 0.179 mmol/g. These results indicate that ZrO_2 is more acidic than CeO_2. Incorporation of ZrO_2 into the CeO_2 lattice enhances the acidity of the support. The alkali impregnated supported Pd catalyst (Na–Pd/CeO_2–ZrO_2) did not show NH_3 desorption peak. In other words, alkali impregnation suppressed the acidity of the catalysts.

3.1.6 Temperature-Programmed Reduction

The H_2 consumption profiles during temperature-programmed reduction (TPR) of supported Pd catalysts are shown in Fig. 7. According to the published reports [19, 38], PdO on ceria–zirconia supports is reduced at low temperatures (60–90 °C). Hence, the H_2 consumption profiles of the present samples were recorded from room temperature onwards up to 950 °C. The interaction of hydrogen with Pd–ceria based catalyst system is very complex as (1) Pd can be reduced at temperatures as low as room temperature, (2) Pd forms hydrides with complex and unknown stoichiometry, (3) the amount of hydrogen stored in these PdH_x depends on their size, and (4) these hydrides, except the surface Pd–H ones, decompose at around 70–80 °C, H spillover occurs on ceria or ceria–zirconia [39]. Indeed Pd/CeO_2–ZrO_2 sample showed such a complicated TPR profile (Fig. 7). The peaks at around 52 °C could be attributed to reduction of PdO. The negative peaks at higher temperatures (100–179 °C) are attributed to decomposition of PdH_x species. Two intense peaks observed 337 and 449 °C are attributed to reduction of surface and bulk ceria. Neat CeO_2 shows reduction peak at around 550 °C [37]. Its shift to low temperature (337 °C) as observed in the present study is due to interaction with zirconia in the solid solution and hydrogen spillover and metal (Pd)-support interactions [37]. When Na is also present the reduction peak due to Pd shifted to higher temperatures (Fig. 7). Reduction of PdO occurred at 61 and 97 °C in Na–Pd/CeO_2–ZrO_2 instead of 52 °C in Pd/CeO_2–ZrO_2. This shift in the reduction peak to higher temperature is a consequence of metal support interactions. Thus, Na impregnation not only alters the textural and acidic properties but also influences the reduction behaviour. The peaks due to CeO_2 reduction which occurred at 337–449 °C in Pd/CeO_2–ZrO_2 are not seen in the case of Na–Pd/CeO_2–ZrO_2. H_2 uptakes exclusively by palladium in Pd/CeO_2–ZrO_2 and Na–Pd/CeO_2–ZrO_2 were estimated to be 0.076 and 0.583 mmol/g, respectively. The higher amount of H_2 consumption in Na–Pd/CeO_2–ZrO_2 than in Pd/CeO_2–ZrO_2 indicates higher dispersion of palladium in the former catalyst. The H_2 consumption for Na–Pd/CeO_2–ZrO_2

Fig. 6 NH_3-TPD profiles of supports and supported Pd catalyst

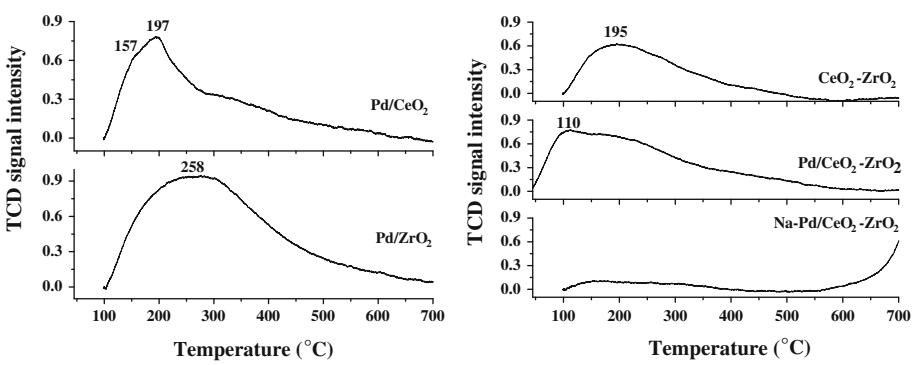

is higher (0.583 mmol/g) than that expected for theoretical PdO reduction (0.188 mmol/g). This difference may be attributed to concurrent reduction of surface Ce^{4+}, which occurs at this lower temperature [40].

3.2 Catalytic Activity

Hydrogenation of cinnamaldehyde (CA) yields different products as shown in Scheme 1. Hydrogenation of the carbonyl group (1,2-addition) yields the unsaturated alcohol—cinnamyl alcohol (CAL). Hydrogenation of the olefinic bond (3,4-addition) gives the saturated aldehyde—hydrocinnamaldehyde (HCA). The 1, 4-addition gives enol which isomerizes into HCA. Further hydrogenation leads to the formation of 3-phenylpropanol (PPL) and subsequently, propylbenzene (PB). Also CAL can get reduced to PPL. Hydrogenation of α, β unsaturated aldehydes on metal surfaces proceeds via the Horiuti–Polayni mechanism involving adsorbed states: di-σC = Oη^2, di-σC = Cη^2, or di-$\pi\eta^2(\eta^4)$ [41–43]. In the present study, over Pd/CeO_2–ZrO_2 catalysts, 3,4 and 1,4-additions are more predominant than the 1,2-addition. At our reaction conditions, formation of PB could not be detected.

3.2.1 *Influence of Support*

The type and the nature of the support have a marked influence on CA conversion and product selectivity (Table 3). CA conversion is higher with Pd supported on ZrO_2 than on CeO_2 (compare entry nos. 4 and 5; Table 3). In the case of Pd supported on CeO_2–ZrO_2, an increase in conversion of CA was observed with increasing amount of ZrO_2 in the mixed oxide composition (compare entry nos. 1 and 3, Table 3). However, PPL selectivity (obtained via hydrogenation of carbonyl group) was relatively higher over Pd supported on CeO_2 (18%) than on ZrO_2 (11.3%). Even in the case of CeO_2–ZrO_2 catalysts, the PPL selectivity was found higher when there is an increase in the composition of CeO_2 in the mixed oxide. In other words, while ZrO_2 support leads to higher conversion and HCA product formation (via 3,4 and 1,4 additions), CeO_2 support results in higher amount of PPL formation. CeO_2 is an easily reducible oxide and hence a part of Pd can be in $\delta+$ state. On the other hand, Pd on ZrO_2 (a weakly reducible oxide) will be in zero state only. An electron depleted $Pd^{\delta+}$ on CeO_2 will polarize the electron rich carbonyl group instead of electron deficient olefinic group and thereby results in preferential 1,2-addition of hydrogen and formation of PPL. $Pd^{\delta+}$ would be less reactive than Pd^0 and hence lower conversion of CA was observed over Pd/CeO_2 than over Pd/ZrO_2.

Table 3 Hydrogenation of cinnamaldehyde over supported Pd catalysts

Catalyst (Ce:Zr molar ratio)	CA conversion (wt%)	Product selectivity (%)		
		HCA	PPL	Others
Pd/CeO_2–ZrO_2 (1:1)	69.6	82.5	16.7	0.7
Pd/CeO_2–ZrO_2 (1:2)	68.1	86.0	13.9	0.1
Pd/CeO_2–ZrO_2 (1:4)	79.6	90.0	10.0	0
Pd/CeO_2	91.0	82.0	18.0	0
Pd/ZrO_2	95.5	88.7	11.3	0

Reaction conditions: Catalyst (0.05 g), cinnamaldehyde (CA, 4 g), solvent—toluene (40 mL), H_2 pressure = 20 bar, reaction time = 8 h. *HCA* hydrocinnamaldehyde, *PPL* 3-phenylpropanol, other products include ethers and acetals

3.2.2 *Effect of Temperature*

Hydrogenation of CA increased with increasing reaction temperature (Table 4). Complete conversion of CA was observed at 80 °C itself. Hydrocinnamaldehyde (HCA) was the major product (82.5–90%). 3-Phenylpropanol (PPL) was detected with selectivity in the range 10.0–16.7%. A small amount of other products including ethers and acetals (0–0.7 wt%) was also detected. With increasing temperature the selectivity of HCA increased at the expense of PPL and other products.

3.2.3 *Effect of Solvent*

The reaction was conducted in non-polar toluene and cyclohexane and polar ethanol solvents (Table 4). In general, CA conversion is much higher in ethanol than in toluene and cyclohexane. Figure 8 shows the conversion verses time plots in different solvents. While HCA is the selective product (82.5–84.6%) in non-polar solvents, HCA (50.7%) along with significant amounts of PPL (10.8%) and other products (acetals + ethers; 38.5%) formed in polar ethanol solvent. Unlike in non-polar solvents, hydrogenation of the carbonyl group of CA yielding PPL is more pronounced in ethanol. As PPL is formed in higher amounts, it participates in further reactions at higher temperatures leading to acetals and ethers (selectivity = 38.5% at 50 °C and 74% at 150 °C).

H_2 pressure influenced CA conversion and products selectivity (Table 5; Fig. 9). The conversion of CA increased from 59.1 to 89.9% by increasing the pressure from 2 to 20 bar. Also a significant reduction in the formation of other products (from 73.6 to 38.5%) was observed at higher temperatures. The reaction occurs even on "bare" CeO_2–ZrO_2. But CA conversion and HCA and PPL selectivity were much higher when Pd was also present. Pd to some extent blocks the acidic sites leading to side reactions on the CeO_2–ZrO_2 surface and thereby enhances the selectivity of the desired products.

Table 4 Influence of temperature on hydrogenation of cinnamaldehyde over Pd (2 wt%)/CeO_2–ZrO_2 (Ce:Zr molar ratio = 1:1)

Temperature (°C)	Solvent = toluene, additive = nil				Solvent = ethanol, additive = nil				Solvent = ethanol, additive = 16 mg NaOH in 10 mL water			
	CA conversion (wt%)	Product selectivity (%)			CA conversion (wt%)	Product selectivity (%)			CA conversion (wt%)	Product selectivity (%)		
		HCA	PPL	Others		HCA	PPL	Others		HCA	PPL	Others
50	69.6 (60.4)[a]	82.5 (84.6)[a]	16.7 (15.0)[a]	0.7 (0.4)[a]	89.9	50.7	10.8	38.5	99.4	67.3	29.7	2.9
80	100	87.7	11.6	0.7	100	37.0	19.9	43.1	100	60.1	32.7	7.3
120	100	88.1	11.3	0.6	100	21.0	14.5	64.5	100	42.1	30.7	27.2
150	100	90.0	10.0	0	100	12.3	12.3	74.0	100	29.5	37.9	32.6
150									100[b]	35.0[b]	40.4[b]	23.3[b]
150									100[c]	20.0[c]	63.4[c]	16.6[c]

Reaction conditions: Catalyst (0.05 g), cinnamaldehyde (CA, 4 g), solvent (40 mL), H_2 pressure = 20 bar, reaction time = 8 h. *HCA* hydrocinnamaldehyde, *PPL* 3-phenylpropanol, other products include ethers and acetals

[a] Data in parentheses corresponds to experiments in cyclohexane instead of toluene

[b] H_2 pressure = 10 bar, additive = 18 mg of NaOH in 30 mL water

[c] H_2 pressure = 10 bar, additive = 54 mg of NaOH in 30 mL water

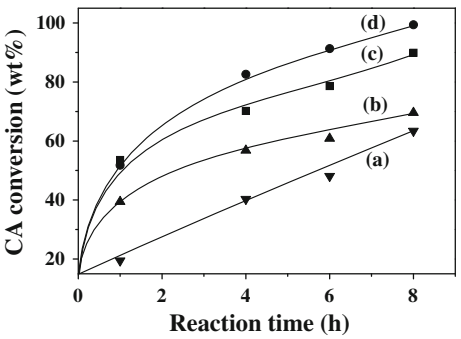

Fig. 8 Conversion versus time plots for hydrogenation of cinnamaldehyde (CA) in different solvents. (*a*) Cyclohexane, (*b*) toluene, (*c*) ethanol and (*d*) ethanol + additive (10 mg of NaOH in 10 mL water). *Reaction conditions*: Pd (2 wt%)/CeO_2–ZrO_2 (Ce:Zr molar ratio = 1:1) = 0.05 g, CA = 4 g, solvent = 40 mL, H_2 pressure = 20 bar, reaction temperature = 50 °C

Table 5 Effect of pressure and alkali on hydrogenation of cinnamaldehyde over Pd (2 wt%)/CeO_2–ZrO_2 (Ce:Zr molar ratio = 1:1)

Catalyst	H_2 pressure (bar)	CA conversion (wt%)	Product selectivity (%)		
			HCA	PPL	Others
CeO_2–ZrO_2	20	58.8	30.4	4.3	65.3
Pd/CeO_2–ZrO_2	20	89.9	50.7	10.8	38.5
	10	86	39.2	9.5	51.3
	5	62.6	38.4	8.8	52.8
	2	59.1	24.5	1.9	73.6
Na–Pd/CeO_2–ZrO_2	20	72.3	89.0	8.9	2.1

Reaction conditions: Catalyst (0.05 g), cinnamaldehyde (CA, 4 g), solvent—ethanol (40 mL), reaction temperature = 50 °C, reaction time = 8 h. *HCA* hydrocinnamaldehyde, *PPL* 3-phenylpropanol, other products include ethers and acetals

3.2.4 *Effect of Alkali Addition*

The formation of acetals and ethers (other products) are catalyzed by acid sites on the catalyst surface. Pyridine-IR (Fig. 5) and NH_3-TPD (Fig. 6) experiments revealed the presence of Lewis acid sites on CeO_2–ZrO_2-based catalysts. In order to suppress these side reactions forming undesired products we have impregnated the catalysts with alkali and then calcined to prepare Na–Pd/CeO_2–ZrO_2. NH_3 desorption is little (0.034 mmol/g) from Na–Pd/CeO_2–ZrO_2 indicating that the catalyst is nearly neutral. The selectivity for the acetals and ethers decreased from 38.5 to 2.1% by using this alkali-modified catalyst (Table 5).

In other experiments, we have added NaOH solution of different concentrations to the reactions over Pd/CeO_2–ZrO_2 in ethanol conducted at 150 °C and 10 bar H_2 pressure (Table 4). Suppression of other products and change in selectivity for hydrogenation of C=C (yielding HCA) to C=O (yielding PPL) was noted. An enhancement in PPL product selectivity from 37.9 to 63.4% was observed when 54 mg of NaOH in 30 mL water was added. Alkali has a positive effect on the rate of hydrogenation (Fig. 8). It activates the C=O group of α, β-unsaturated aldehydes and facilitates hydrogenation yielding unsaturated alcohols (CAL). The enhanced activation of the C–O bond could be interpreted by the polarization of C=O bond resulting from the interaction of the alkali cation with the lone-pair electrons of the oxygen atom of the C–O group. These unsaturated alcohols (CAL) are further hydrogenated to saturated alcohols (PPL) in presence of Pd/CeO_2–ZrO_2 catalyst by 1,4

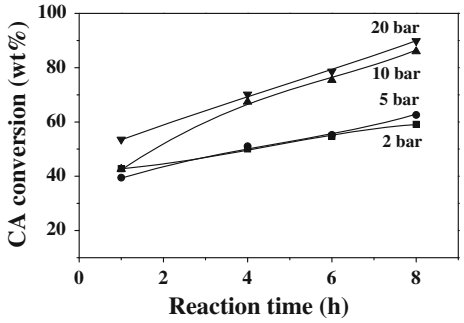

Fig. 9 Conversion of cinnamaldehyde (CA) at various pressures over Pd (2 wt%)/CeO_2–ZrO_2 (Ce:Zr molar ratio = 1:1) catalyst. *Reaction conditions*: catalyst = 0.05 g, CA = 4 g, ethanol = 40 mL, reaction temperature = 50 °C

addition. Finally, the saturated alcohol percentage increases with increasing alkali percentage and the formation of acetals and ethers is reduced. Mahmoud et al. [2] reported that hydrogenation of HCA to PPL does not occur significantly at normal temperatures over Pd/SiO_2 catalyst. However, the hydrogenation of CAL proceeds very fast (30 times faster than the hydrogenation of CA to CAL) [2]. These sequential reactions thereby enhance the selectivity of PPL in the product. A similar behaviour occurs even in our experiments. The Na ions in Na–Pd/CeO_2–ZrO_2 are involved mainly in the reduction of acid sites on the support surface. On the other hand, in the experiments with alkali solutions, the alkali ions have not only suppressed the acidity of the catalyst but at the same time involved in polarising the C=O group of CA leading to differences in product selectivity.

The catalytic activity of Pd (2 wt%)/CeO_2–ZrO_2 is significantly higher than that of carbon nanofiber and activated carbon-supported Pd (5 wt%) catalysts. With less amount of Pd in the former catalyst, complete conversion of CA at 80 °C was achieved in just 1 h while it requires nearly 30 h over the latter catalysts [44]. Pd (1 wt%)/SiO_2 required higher temperature (100 instead of 80 °C), pressure (30 instead of 20 bar) and amount of catalyst (200 instead of 50 mg) to achieve similar conversions of CA. In other words, the Pd catalysts of the present study are more efficient and the support has a significant role in the improved activity of these catalysts. Pd catalysts are known for selective hydrogenation of C=C. However, in this study, it is demonstrated that by adding a small quantity of alkali, the electronic and redox properties of Pd can be fine-tuned and the selectivity for hydrogenation (between C=C and C=O of cinnamaldehyde) can be controlled.

4 Conclusions

Chemoselective hydrogenation of cinnamaldehyde over CeO_2–ZrO_2 supported Pd catalysts is reported for the first time. Cinnamaldehyde has two functional groups (C=C and C=O) for hydrogenation. In general, the hydrogenation of C=C is preferred over Pd catalysts. However, by adding a small quantity of alkali the selectivity for hydrogenation can be changed/altered. Alkali addition influenced the dispersity, electronic property and reducibility of Pd. These changes in molecular electronic structure of Pd are responsible for the changes in the chemoselectivity brought about by alkali addition.

Acknowledgments S.B. acknowledges the Council of Scientific and Industrial Research, New Delhi for the award of Junior Research Fellowship. Authors thank Dr. K.V.R. Chary, IICT, Hyderabad for the help in TPR measurements.

References

1. Boudart M (1994) Nature 372:320
2. Mahmoud S, Hammoudeh A, Gharaibeh S, Melsheimer J (2002) J Mol Catal A 178:161
3. Serrano-Ruiz JC, Luettich J, Sepúlveda-Escribano A, Rodríguez-Reinoso F (2006) J Catal 241:45
4. Kluson P, Cerveny L (1995) Appl Catal 128:13
5. Chen XF, Li HX, Xu YP, Wang MH (2002) Chin Chem Lett 13:107
6. Claus P, Brülckner A, Mohr C, Hofmeister H (2000) J Am Chem Soc 122:11430
7. Rylander PN (1979) Catalytic hydrogenation in organic synthesis. Academic Press, New York, p 72
8. Zhang L, Winterbottom JM, Boyes AP, Raymahasay S (1998) J Chem Technol Biotechnol 72:264
9. Delbecq F, Sautet P (1995) J Catal 152:217
10. Ranga Rao G, Kašpar J, Di Monte R, Meriani S, Graziani M (1994) Catal Lett 24:107
11. Zhao B, Li G, Ge C, Wang Q, Zhou R (2010) Appl Catal B 96:338
12. Shen M, Wang J, Shang J, An Y, Wang J, Wang W (2009) J Phys Chem C 113:1543
13. Shen M, Yang M, Wang J, Wen J, Zhao M, Wang W (2009) J Phys Chem C 113:3212
14. Graham GW, Jen HW, McCabe RW, Straccia AM, Haack LP (2000) Catal Lett 67:99
15. Zhao M, Chen S, Zhang X, Gong M, Chen Y (2009) J Rare Earths 27:728
16. Bera P, Patil KC, Jayaram V, Subbanna GN, Hegde MS (2000) J Catal 186:293
17. Specchia S, Palmisano P, Finocchio E, Busca G (2010) Chem Eng Sci 65:186
18. Wang G, Meng M, Zha Y, Ding T (2010) Fuel. doi:10.1015/j.fuel.2010.03.031
19. Wang H, Chen Y, Zhang Q, Zhu Q, Gong M, Zhao M (2009) J Nat Gas Chem 18:211
20. Velu S, Kapoor MP, Inagaki S, Suzuki K (2003) Appl Catal A 245:317
21. Vivier L, Duprez D (2010) ChemSusChem 3:654
22. Yashima M, Hirose T, Katano S, Suzuki Y, Kakihana M, Yoshimura M (1995) Phys Rev B 51:8018
23. Otsuka-Yao-Matsuo S, Omata T, Izu N, Kishimoto H (1998) J Solid State Chem 138:47
24. Omata T, Kishimoto H, Otsuka-Yao-Matsuo S, Ohtori N, Umesaki N (1999) J Solid State Chem 147:573
25. Thomson JB, Armstrong AR, Bruse PG (1996) J Am Chem Soc 118:11129

26. Montini T, Speghini A, De Rogatis L, Lorenzut B, Bettinelli M, Graziani M, Fornasiero P (2009) J Am Chem Soc 131:13155
27. Shah PR, Kim T, Zhou G, Fornasiero P, Gorte RJ (2006) Chem Mater 18:5363
28. Montini T, Hickey N, Fornasiero P, Graziani M, Bañares MA, Martinez-Huerta MV, Alessandri I, Depero LE (2008) Chem Mater 17:1157
29. Montini T, Bañares MA, Hickey N, Di Monte R, Fornasiero P, Kašpar J, Graziani M (2004) Phys Chem Chem Phys 6:1
30. Trovarelli A (1996) Catal Rev 38:439
31. Li G, Zhao B, Wang Q, Zhou R (2010) Appl Catal B 97:41
32. Martínez-Arias A, Fernández-García M, Ballesteros V, Salamanca LN, Conesa JC, Otero C, Soria J (1999) Langmuir 15:4796
33. Franchini CA, Cesar DV (2010) Catal Lett 137:45
34. Dolbecq A, Compain JD, Mialane P, Marrot J, Secheresse F, Keita B, Holzie LRB, Miserque F, Nadjo L (2009) Chem Eur J 15:733
35. Parvulescu VI, Parvulescu V, Endruschat U, Filoti G, Wagner FE, Kubel C, Richards R (2006) Chem Eur J 12:2343
36. Roy S, Marimuthu A, Hegde MS, Madras G (2008) Catal Commun 9:811
37. Bekyarova E, Fornasiero P, Kašpar J, Graziani M (1998) Catal Today 45:179
38. Luo MF, Zheng XM (1999) Appl Catal A 189:15
39. Gatica JM, Baker RT, Fornasiero P, Bernal S, Kašpar J (2001) J Phys Chem B 105:1191
40. Formasiero P, Di Monte R, Ranga Rao G, Kašpar J, Trovarelli A, Graziani M (1995) J Catal 151:168
41. Bauer K, Garbe D (1985) Common fragrance and flavor materials. VCH, Weinheim
42. Fukuzawa SI, Fujuami T, Yamuchi S, Sakai S (1986) J Chem Soc Perkin Trans I 1929
43. Touroude R (1980) J Catal 65:110
44. Pham-Huu C, Keller N, Ehret G, Charbonniere LJ, Ziessel R, Ledoux MJ (2001) J Mol Catal A 170:155